ChemElectroChem

Research Article
doi.org/10.1002/celc.202500034

Chemistry Europe
European Chemical Societies Publishing

www.chemelectrochem.org

Feed and Bleed Operating Mode for Electrochemical Flow Cells: Challenges, Solutions and Practical Insights

Jonas Baessler,[a] Malte Wehner,[a] Mojtaba Mohseni,[a] Julian Neumann,[a] Matthias Wessling,[a, b] and Robert Keller*[a]

Electrochemical processes offer promising routes to defossilize the chemical industry by integrating low-carbon electricity. However, bridging the gap between lab-scale experimental studies and pilot-scale industrial applications is still challenging: Lab-scale electrochemical flow cells typically operate in batch or single-pass mode, with each mode facing limitations regarding the steady-state operation at industrially relevant conditions. This work introduces the "feed and bleed" operating mode with continuous exchange of a recirculated electrolyte stream, which enables versatile steady-state operation. The "feed and bleed" mode is compared to batch and single-pass operation. We develop a mathematical model for "feed and bleed" operation and validate the model experimentally. Additionally, this work introduces a 3D-printed phase separator coupled with lab-scale flow cells to separate gas from the recirculated liquid stream. Batch, single-pass, and "feed and bleed" operation are demonstrated by methanol oxidation to formate at 200 mA/cm^2 in a 25 cm^2 flow cell. This provides an experimental comparison concerning product/reactant concentration, conversion, and Faraday efficiency. The comparison highlights the characteristics of each operation mode for the electrosynthesis of chemicals, showcasing the unique characteristics of the feed and bleed mode, which enables steady-state operation at industrially-relevant conditions with high product concentration.

1. Introduction

Despite all the entailing challenges, the transition from a fossil-based industry to a renewable-based industry has opened new windows and avenues toward modern chemical engineering. Within this contemporary landscape, electrochemistry and electrochemical engineering domains stand out as pivotal contributors.[1,2] Their significance lies in harnessing the power of electricity as the primary driving force, which aligns with the potential of renewable energies.[3–5]

Nevertheless, electrochemical studies often remain confined to fundamental research at low current density and low product concentration, focusing more on initial selectivity than long-term stability. While fundamental studies are important, investigating electrochemical synthesis at industrially relevant conditions is imperative to proceed from laboratory towards application.[6–8] For industrial electrolysis, predominantly flow cells are used because they enable continuous production processes and controlled flow regimes, e.g., for chlor-alkali or water electrolysis.[9,10] Flow cells are preferable to beakers or H-cells at lab-scale since they also represent industrial conditions, facile scale-up, and provide well-defined and reproducible conditions.[11–13]

Although the influence of reaction conditions and the cell setup are often discussed,[8,14–20] the operating mode of the flow cells received less consideration. Electrochemical flow cells at lab-scale are typically operated in two modes: batch or single-pass.[12,21,22] In batch mode (also known as semi-batch or batch recirculation),[13,23] the electrolytes are circulated through the cell in a closed loop.[24] High product concentrations can be obtained over time;[13] however, batch mode is unsuitable for continuous synthesis in steady-state. In single-pass mode (see also continuous flow or flow electrochemistry),[23,25,26] the electrolyte is passed through the cell only once, which readily enables steady-state operation.[24] Nonetheless, achieving a high product concentration in the single-pass mode sets constraints on the flow channel geometry and the flow rate.[27] Due to their specific characteristics, neither batch nor single-pass are suitable to investigate continuous production in flow cells that resemble industrially relevant conditions regarding product concentration, cell geometry and flow velocity.

Beyond batch and single-pass, a third operating mode is commonly employed for continuous production in industrial electrosynthesis,[28–31] electrodialysis and filtration,[32–34] which was coined "feed and bleed" in the field of membrane technology[32–34] (see also "continuous reactor with recycle").[29] In feed and bleed mode, the electrolyte is circulated in a loop at a high flow rate through the flow cell. Concurrently, a small volume flow enters the loop (Feed), while an equivalent volume

[a] J. Baessler, M. Wehner, M. Mohseni, J. Neumann, M. Wessling, R. Keller
RWTH Aachen University
Aachener Verfahrenstechnik – Chemical Process Engineering
Forckenbeckstr. 51
52074 Aachen, Germany
E-mail: robert.keller@avt.rwth-aachen.de

[b] M. Wessling
DWI – Leibniz Institute for Interactive Materials
Forckenbeckstr. 50
52074 Aachen, Germany

Supporting information for this article is available on the WWW under https://doi.org/10.1002/celc.202500034

flow leaves the loop (Bleed).[32] In industrial organic electrosynthesis the recirculation often involves one or more separation steps to obtain a purified product stream while the remaining electrolyte is recycled.[30,31] In contrast to batch and single-pass mode, feed and bleed allows continuous production in steady state at high product concentration without setting constraints to the flow conditions within the cell. While "feed and bleed" is commonly employed in industrial electrosynthesis, it is only scarcely used to study electrochemical reactions at lab-scale.[35–37]

This work provides valuable tools and insights for the feed and bleed operation mode in lab-scale electrosynthesis, and discusses its unique characteristics in direct comparison with batch and single-pass mode (see schematic illustrations in Figure 1). We introduce equations for modeling and evaluating feed and bleed systems and discuss influencing factors such as the feed flow rate and the electrolyte volume. Additionally, we highlight the significance of gas separation from the recycle stream for the feed and bleed operation, which is effectively achieved with a 3D-printed phase separator. Furthermore, we present an experimental setup for feed and bleed mode that can also be operated in batch and single-pass mode. Online FTIR analysis monitoring the product concentration provides quantitative insights into the specific characteristics of the flow cell operating modes. We demonstrate feed and bleed operation at lab-scale and directly compare with batch and single-pass at the example of methanol oxidation to formate in a flow cell with an active electrode area of 25 cm^2 at a current density of 200 mA/cm^2. With this work, we facilitate the adoption of "feed and bleed" for lab-scale research, providing valuable tools for investigating electrosynthesis under industrially relevant conditions and assessing long-term stability during steady-state operation.

2. Results and Discussion

2.1. Feed and Bleed System Behavior

The feed and bleed system can be considered as an ideally mixed volume at high recirculation flow rates, as shown in Figure 2. A comparison of the ideally mixed model with a non-ideally mixed model is provided in the Supporting Information (Figures S1–S3), indicating that the assumption of ideal mixing

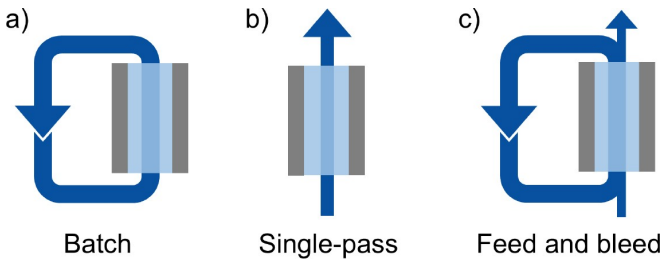

Figure 1. Schematic representation of the three operation modes for electrochemical flow cells.

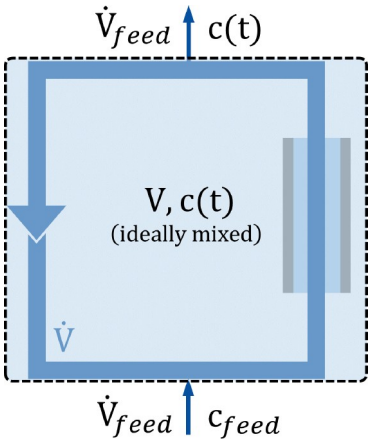

Figure 2. Model of the feed and bleed setup assuming ideal mixing for the total electrolyte volume in the system.

is justified for typical feed and bleed operation with high recirculation rate.

The ideally mixed model can be described by a mole balance around the feed and bleed system as shown in Equation (1). The mole balance describes the change in product concentration $c(t)$ in the ideally mixed electrolyte volume V depending on the volume flow rate of the feed $\dot{V}_{feed}$, the product concentration in the feed c_{feed} and the electrochemical reaction with the current density i, the geometric electrode area A, the Faraday efficiency FE, the number of electrons transferred to form the product z, and the Faraday constant F. In the following equations and calculations, we assume that the product concentration in the feed and the initial product concentration in the electrolyte are both zero ($c_{feed} = c_0 = 0\ mol\,L^{-1}$), which corresponds to our experimental conditions and most electrosynthesis applications.

$$V\frac{dc(t)}{dt} = \dot{V}_{feed}(c_{feed} - c(t)) + \frac{iA \cdot FE}{zF} \quad (1)$$

Besides the electrochemical reaction, the system behavior is governed by the electrolyte volume in the system and the feed flow rate. The effect of both parameters on the product concentration is illustrated in Figure 3, starting at t = 0 when the current is switched on and a faradaic reaction to a product begins. The concentration curves can be described by Equation (2), which is the analytical solution of the mole balance (Equation (1)). The feed flow rate $\dot{V}_{feed}$ determines the rate at which the electrolyte solution in the system is replaced, which allows the adjustment of the obtainable product concentration (and thus conversion) at steady-state as shown in Figure 3a.

Reducing the feed flow rate from 5 to 2.5 $mL\,min^{-1}$ doubles the steady-state concentration in agreement with Equation (3). However, lowering the feed flow rate increases the time until steady state is reached. In this work, the transient phase refers to the period in which the product concentration is < 98 % of the steady-state value. The duration of the transient phase t_{98}

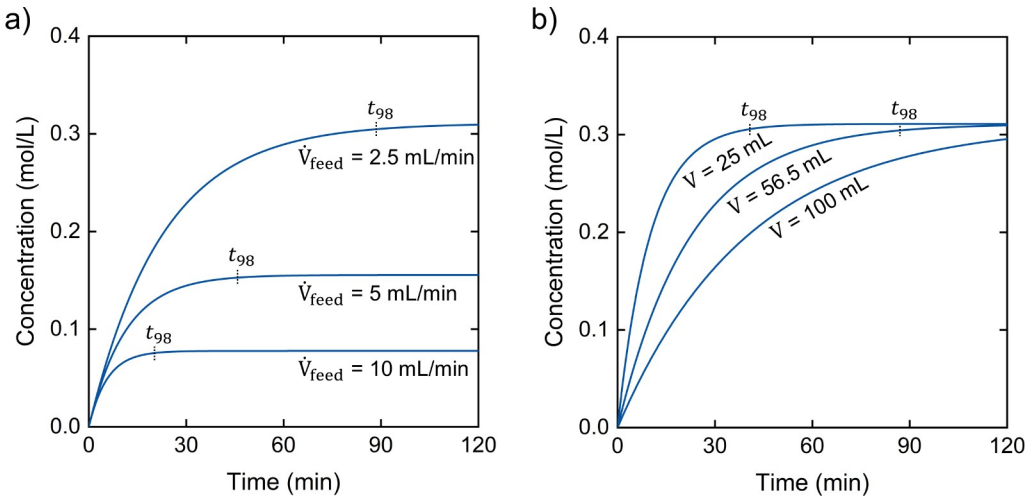

Figure 3. Product concentration curves of feed and bleed systems calculated with the ideally mixed model, starting at t = 0 when the current is switched on and a faradaic reaction begins. The plots show the influence of (a) the volume flow of the feed and (b) the total electrolyte volume in the system. The varied parameters are indicated in each plot. All other parameters remained unchanged at the values of our experimental setup ($\dot{V}_{feed}$ = 2.5 mL min^{-1}, V = 56.5 mL, i = 200 mA cm^{-2}, A = 25 cm^2, FE = 100 %, and z = 4 electrons transferred per reaction).

can be calculated according to Equation (4), which was derived from the ideally mixed model.

$$c(t) = \frac{iA \cdot FE}{zF\dot{V}_{feed}} \cdot (1 - \exp(-\frac{\dot{V}_{feed}}{V} \cdot t)) \quad (2)$$

$$c(t \to \infty) = \frac{iA \cdot FE}{zF\dot{V}_{feed}} \quad (3)$$

$$t_{98} = -V/\dot{V}_{feed} \cdot \ln(1 - 0.98) \quad (4)$$

The transition time increases proportional to the electrolyte volume V of the system, as shown in Figure 3b. A low volume is advantageous in enabling the system to respond quickly and reach a steady state faster.

The Faraday efficiency (FE) is one of the most important metrics in electrochemical synthesis. Equations for FE calculation from discrete points of product concentration are presented for different operating modes in Table 1. In comparison to the straightforward FE calculation for batch or single-pass mode (see Equations (5) and (6)), the specific behavior of the feed and bleed system must be considered to evaluate the FE from measured product concentration data correctly. Feed and bleed operation in a steady state resembles the single-pass mode (compare Equations (3) and (6)); however, the use of Equation (6) for the feed and bleed mode does not allow for accurate FE calculation in the transient phase. To overcome this limitation, we derived Equation (7) from the ideally mixed model to calculate the FE during the entire feed and bleed operation.

If the internal volume and the feed flow rate are known, the FE of the product-forming reaction can be calculated from discrete points of the product concentration, as demonstrated in Figure 4. Figure 4a displays discrete concentrations of a curve calculated for a constant FE of 100 %. Calculating the FE from the discrete concentration points matches the true FE of the calculated concentration curve exactly, as shown in Figure 4b. The proposed equation for FE calculation allows for determining the FE from discrete concentration measurements during both the transient phase and steady state. In addition to the validated model-based FE calculation, we validated the approach experimentally, as shown in the Supporting Information (Figure S4).

Table 1. Equations for FE calculation from discrete points of product concentration for the different operating modes. The indices n and $n-1$ describe two consecutive discrete points in time.

Mode	Equation	
Batch	$FE_n = \frac{zFV}{iA} \cdot \frac{c_n - c_{n-1}}{t_n - t_{n-1}}$	(5)
Single-pass	$FE_n = \frac{zF\dot{V}_{feed}}{iA} \cdot c_n$	(6)
Feed and bleed	$FE_n = \frac{zF\dot{V}_{feed}}{iA}\left(c_{n-1} + \frac{c_n - c_{n-1}}{1-\exp\left(-\frac{\dot{V}_{feed}}{V}(t_n - t_{n-1})\right)}\right)$	(7)

2.2. Phase Separation in a Feed and Bleed System

Gas evolution is common in many electrochemical processes, often involving hydrogen or oxygen evolution in aqueous electrolytes. Gas evolution might occur as an undesired side reaction or result from the intended reaction (e.g., water electrolysis). It is necessary to remove gas bubbles from the liquid electrolyte to prevent gas accumulation within the recirculation loop. We designed the phase separator shown in Figure 5a for that purpose. The phase separator was 3D-printed with threaded ports for standard tubing connectors. The two-phase stream from the electrochemical cell enters the phase separator on the single inlet on the left side tangentially,

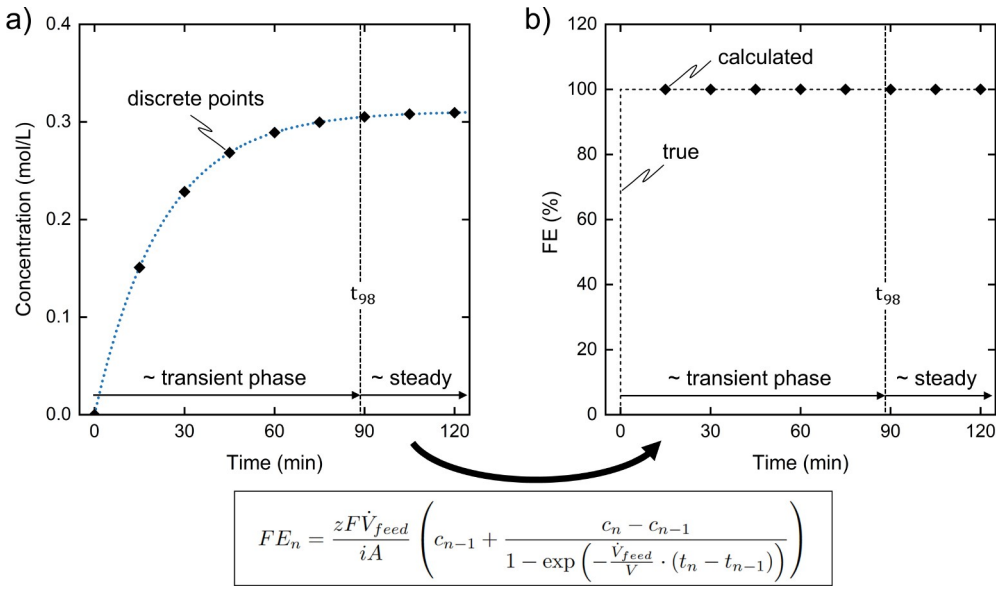

Figure 4. a) Discrete points on a product concentration curve calculated for a constant FE of 100% (blue dotted line). The parameters of our experimental demonstration (see Figure 6) were used for the calculation ($\dot{V}_{feed} = 2.5$ mL min^{-1}, $V = 56.5$ mL, $i = 200$ mA cm^{-2}, $A = 25$ cm^2, and $z = 4$). The end of the transient phase is indicated by a vertical dashed line. b) FE calculated from the discrete concentration points by Equation (7) (also shown in the Figure) compared to the true FE.

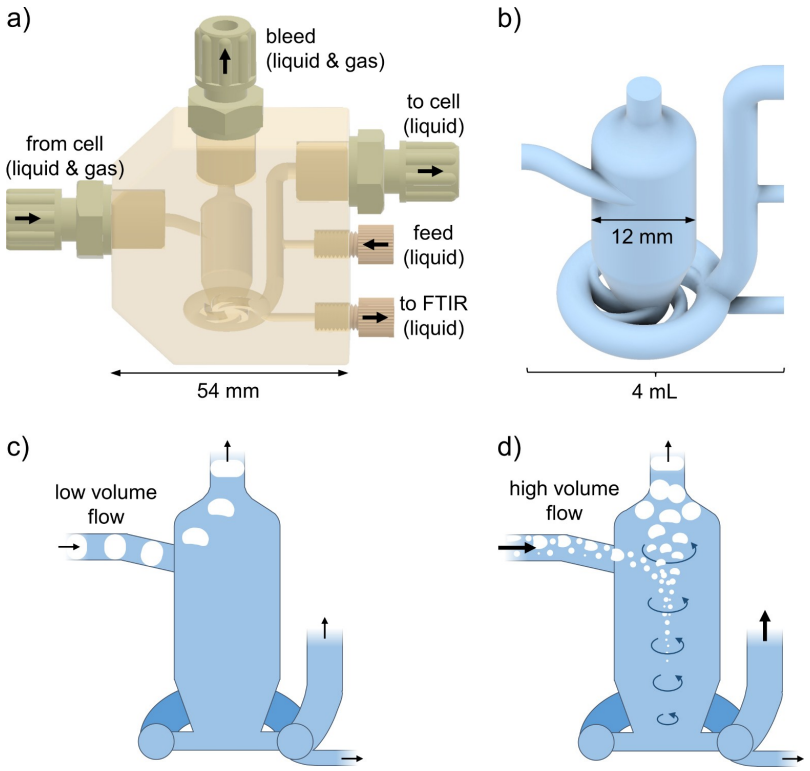

Figure 5. a) CAD image of the phase separator with an inlet on the left side, an overflow outlet at the top, and an analysis outlet, a feed inlet, and a cell stream outlet on the right side. b) Internal channels and separation chamber of the phase separator. c) At low volume flow rates gas bubbles from the electrochemical cell rise to the bleed outlet, d) At high volume flow rates the gas separation is supported by a hydrocyclone-like motion in the central chamber.

resembling a hydrocyclone. Thus, secondary flow is introduced in the central chamber and facilitates bubble removal through the bleed stream at the top. The bubble-free electrolyte flows through tangential outlets at the bottom of the separation chamber towards the outlet on the right side, which mixes with the incoming feed stream. An additional outlet on the bottom

right allows for analysis of the composition of the product stream (see Figure 9 for the experimental setup). The phase separator was designed for a low internal volume and uses two separation principles depending on the volume flow. When the separator was operated at low volume flow (< 20 mL/min), gas bubbles ascended towards the top outlet as illustrated in Figure 5b. This observation indicates that the buoyancy of the gas bubbles was the primary driving force of separation at low-volume flows. With increasing volume flow (> 20 mL/min), gas bubbles were more finely dispersed in the electrolyte, and the centrifugal forces started to contribute to the separation process. This dynamic was facilitated by the tangential inlet design, which imparted a hydrocyclone-like motion to the incoming flow, forcing the gas bubbles to accumulate at the center of the chamber as depicted in Figure 5c. The centrifugal force pushes the liquid electrolyte towards the outer walls of the separation chamber, ensuring that the electrolyte exits through the tangential outlets at the bottom without gas bubbles. The effect of centrifugal forces intensified with increased volume flow, efficiently segregating the gas bubbles from the liquid electrolyte. This mechanism highlights the capability of the phase separator to adapt its separation strategy based on the flow conditions, ensuring effective gas removal despite its low internal volume of 4 mL. Separating gas bubbles can also be achieved by buoyancy alone with a less complex but larger separator made from a simple bottle, as described in the Supporting Information (Figure S6). However, the design of the 3D printed phase separator with low internal volume reduces the time required to reach a steady state and the residence time in the loop. Both of which are beneficial for feed and bleed operation.

2.3. Methanol Oxidation: Comparison of Operation Modes

Electrochemical methanol oxidation is a promising anodic reaction that can provide value-added products while operating at a lower electrode potential than oxygen evolution.[38–42] Methanol oxidation to formate (Equation (8) readily reaches high conversion and product concentration;[43] hence, it has been selected for investigating the operation modes at an industrially relevant current density of 200 mA cm^{-2}. A pre-oxidized copper foam coated with copper dendrites was employed as an anode as described in our previous publication.[43]

$$CH_3OH + 5OH^- \rightarrow HCOO^- + 4H_2O + 4e^- \quad (8)$$

For comparison of the operating modes, we calculated the ideal concentration curves for methanol oxidation to formate in batch, single-pass, and feed and bleed mode (Figure 6a–c) and measured the concentration curves experimentally (Figure 6d–f). A constant FE of 100 % for formate was assumed as the ideal case for the calculation, while a lower FE was determined in the experiments (Figure 6g–i). As in the experiments, the same volume, flow rate, and current density were used for the calculation. All experiments were carried out with the same experimental setup, which can be used for all three operating modes depending on the pump settings (see Figure S5).

In ideal batch mode at constant FE, the reactant concentration decreases linearly while the product concentration increases linearly, as depicted in the calculated concentration curves in Figure 6a. With increasing experiment duration, an increasing amount of methanol is converted to formate. Compared to ideal reactor models in chemical reaction engineering, the behavior of a flow cell in batch mode with closed recirculation corresponds to an ideal batch reactor (stirred tank), as both represent a closed system. The slope of the changing concentrations depends on the current density i, the electrode area A, the FE, the number of electrons transferred per reaction z, and the electrolyte volume V in the batch setup.

During methanol oxidation with our setup operating in batch mode, we observed a nearly linearly decreasing methanol concentration as shown in Figure 6d, in agreement with the model prediction. However, the formate concentration in the experiment increased with decreasing slope, reaching a maximum concentration of 0.44 mol/L. Comparing experimental (d) and calculation data (a) suggests a decreasing FE over time for formate formation since its concentration does not follow a linear increasing trend throughout the experiment. The FE correlates with the slope of the formate concentration and is calculated with Equation (5) from the change in formate concentration between two time points. Figure 6g illustrates the decreasing FE and increasing methanol conversion over time determined from the concentration data of the experiment. Although FE for formate formation was above 90 % within the first 5 minutes of the experiment, the FE dropped significantly afterward, reaching 0 % at 56 min. One credible explanation for the decreasing FE is the further electro-oxidation of formate to carbonate, which is a known side product of methanol oxidation on copper oxide.[39,44] Recently, we demonstrated the effect of the ratio of formate to methanol on the FE for anodic oxidation of methanol to formate, elaborating on possible pathways for formate loss.[43]

In batch operation mode, we reached a high conversion of nearly 80 % of the initial 1 mol/L methanol within the experiment duration of less than 60 min. The rapid progress of the oxidation was enabled by the high current density of 200 mA/cm^2 and the high ratio of geometrical electrode area (25 cm^2) to electrolyte volume (56.5 mL). Our results show that the batch operation mode is well suited to achieve high conversion and product concentrations. However, the concentration of reactant and product are constantly changing. Since no steady state is reached, a single batch experiment cannot distinguish temporal effects such as possible deterioration of the electrode from the influence of the increasing reaction progress.

In ideal single-pass mode at constant FE, product, and reactant concentrations are constant after a short transient phase, as shown in the calculated concentration curves in Figure 6b. A flow cell in single-pass mode behaves similarly to an ideal plug flow reactor (PFR), where the reaction

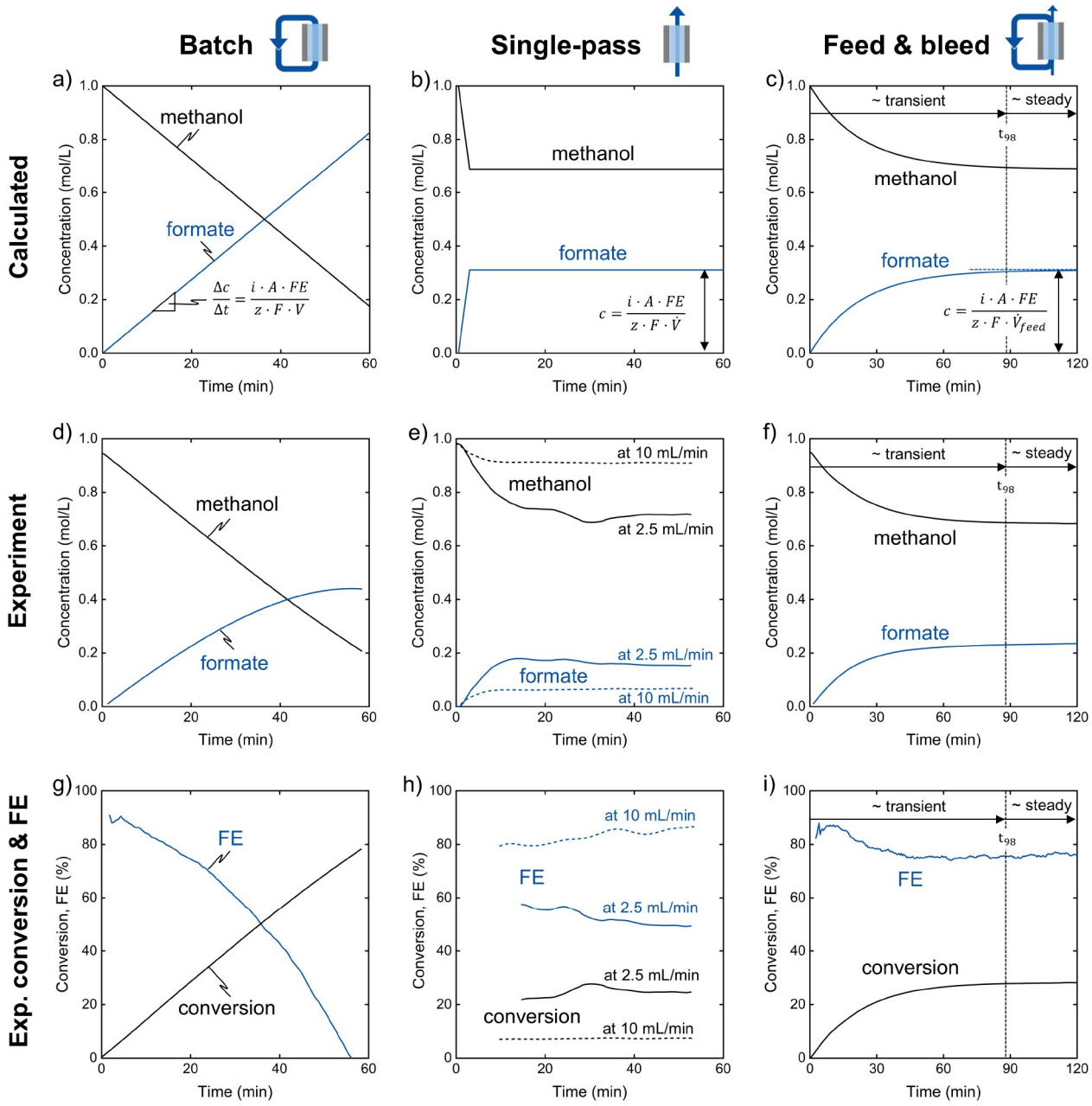

Figure 6. a–c) Ideal concentration curves calculated for methanol oxidation to formate in batch, single-pass, and feed&bleed operation mode with a constant FE of 100%. The calculation was performed with the same volume, flow rate, and current density as the experiments. d–f) Measured concentrations during oxidation experiments in batch ($V = 56.5$ mL, $\dot{V} = 50$ mL min^{-1}), single-pass (two experiments, at $\dot{V} = 2.5$ mL min^{-1} and at $\dot{V} = 10$ mL min^{-1}), and feed&bleed operation mode ($V = 56.5$ mL, $\dot{V}_{cycle} = 50$ mL min^{-1}, $\dot{V}_{feed} = 2.5$ mL min^{-1}). g–i) Methanol conversion and FE for formate determined from the measured concentration data by applying Equations (5)–(7). Experimental conditions: 200 mA cm^{-2}, 25 °C, 2 mol L^{-1} KOH, 1 mol L^{-1} methanol.

progress increases with the distance the flow travels through the reactor. The short transient phase in the calculation is caused by the residence time of the flow in the cell and the time delay until the flow reaches the point of concentration measurement. Assuming an ideal plug flow without back mixing, the transient phase in the calculation is short. The product concentration in single-pass mode is determined by the current density i, the geometric electrode area A, the FE, the number of electrons transferred per reaction z, and the flow rate $\dot{V}$ through the cell. We investigated methanol oxidation in our setup in single-pass mode in two separate experiments at a flow rate of 2.5 mL/min and 10 mL/min. As expected, more methanol was converted to formate at a flow rate of 2.5 mL/min than at 10 mL/min, as shown in the concentration curves in Figure 6e. The transient phase was significantly longer than the ideal calculation, which we attribute to non-ideal flow (back mixing, dead volumes, and recirculated anolyte through the FTIR spectrometer). After the initial transient phase, the concentrations of methanol and formate were fairly constant, with slight fluctuations for

the experiment at 2.5 mL/min. Figure 6h shows FE and conversion over time calculated from the single pass concentration data by Equations (6) and (9). The non-ideal transient phase was not evaluated as the applied FE equation was derived from the ideal system behavior. The experiment at 2.5 mL/min showed a lower FE at higher methanol conversion (49–57 % FE at 22–28 % conversion), compared to the experiment at 10 mL/min (80–86 % FE at 7.0–7.5 % conversion). As observed in the batch experiment, the FE was lower at higher conversion, since an increasing ratio of formate to methanol facilitates the overoxidation of formate to carbonate. However, the lower FE at 2.5 mL/min can be only partially explained by the higher conversion. Figure 7 directly compares the three different operating modes by plotting the FE against the conversion showing that at the same conversion the FE in single-pass mode at 2.5 mL/min was significantly lower than for batch mode at a flow rate of at 50 mL/min. We attribute the difference to an increasing mass transfer limitation with decreasing single-pass flow rate. The flow rate of 2.5 mL/min, required for about 25 % conversion, corresponds to a very low mean flow velocity of 0.24 mm/s in the cell. In single-pass mode, product concentration and mass transfer cannot be investigated separately, as product concentration and mass transfer are directly dependent on the flow rate. In this context, the shape of the channel inside the cell is crucial (cross-section area of the flow and active electrode area). In small meandering microfluidic channels, a flow velocity with sufficient mass transfer can be achieved even at a low flow rate so that a high product concentration can be achieved in single-pass mode.[12] However, in flow cells with a larger cross-section area of the flow, such as the flow cell used in this work (cross-section: 1.75 cm^2), the single-pass mode is unsuitable for high product concentrations due to mass transfer

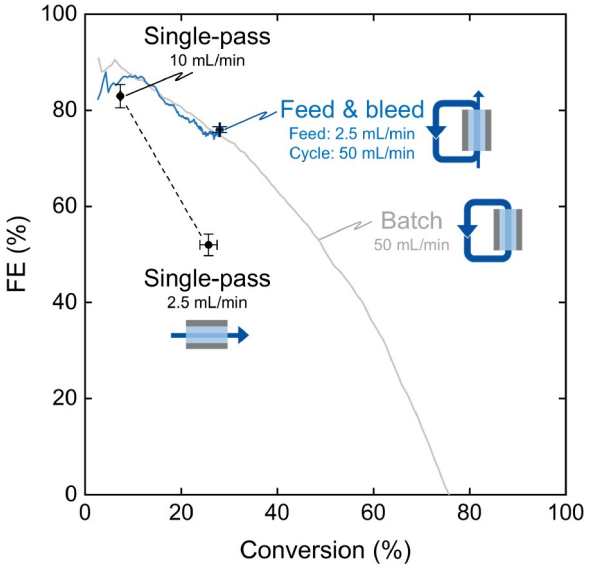

Figure 7. FE for formate plotted over methanol conversion from the data of Figure 6, comparing batch, single-pass, and feed&bleed operating mode. Experimental conditions: 200 mA cm^{-2}, 25 °C, 2 mol L^{-1} KOH, 1 mol L^{-1} methanol.

limitations. A major advantage of the single-pass mode is the operation in a steady state, which is reached quickly with only a short transient phase. Steady-state operation enables long-term experiments and facilitates the investigation of temporal effects such as electrode degradation.

In ideal feed and bleed mode at constant FE, the reactant concentration decreases, and the product concentration increases until a steady state is reached, as depicted in the calculated concentration curves in Figure 6c. In a steady state, the rate of product formation at the electrode equals the product removal rate through the bleed stream. The concentration curves for an electrochemical flow cell in feed and bleed mode present a behavior similar to an ideal continuous stirred-tank reactor (CSTR). For ideal feed and bleed, the product concentration converges to the concentration ideal single-pass would reach at the same feed flow rate (compare equations in Figure 6b and 6c). We consider the system in a steady state when the product concentration reaches 98 % of its final value. The end of the transient phase, when 98 % of the final concentration is reached, is marked by a black dashed line in the plot and was calculated by Equation (4). As described in the equation, the duration of the transient phase depends on the electrolyte volume V in the system and on the feed rate $\dot{V}_{feed}$. During methanol oxidation with our setup operating in feed and bleed mode, we observed concentration curves of methanol and formate that closely resembled the ideal calculation (Figure 6f). However, the formate concentration converged to 0.24 mol/L in our experiment compared to 0.31 mol/L in the calculation that assumed a constant FE of 100 %. The lower formate concentration can be attributed to a FE $<$ 100 %. The FE in feed and bleed mode can be determined from the formate concentration even before a steady state is reached by applying Equation (7). Figure 6g shows the FE and methanol conversion calculated from the concentration data. The initial FE for methanol oxidation was high, reaching up to 88 %. With increasing methanol conversion, the FE converged to 76 % at 28 % conversion at steady state.

If the FE is plotted against conversion as shown in Figure 7, the resulting FE curve of feed and bleed closely aligns with the curve obtained in batch operation. The FE curves deviated slightly at low conversion, likely caused by artifacts of non-ideal mixing and the reduced accuracy of the FTIR analytics at low formate concentration. The difference between the FE at the steady state operating point in feed and bleed mode and in batch mode at the same conversion of 28 % was remarkably low (76 % vs. 74.7 %). The good agreement of batch and feed&bleed FE demonstrates that our calculation method provided accurate FE data for most of the transient phase and the steady state operating point. Furthermore, our results illustrate that feed and bleed can be operated in a steady state at high conversion without mass transfer limitation. In contrast to the single-pass mode, the achievable conversion in feed and bleed mode was successfully decoupled from the flow rate in the cell, as the steady state conversion can be increased by decreasing only the feed flow rate. The feed and bleed mode follows the same relationship of FE and conversion as observed in batch mode (see Figure 7), but in contrast to batch mode, a

single point on the FE-conversion curve can be selected for continuous operation. Therefore, feed and bleed provides a unique opportunity to investigate electrochemical processes at both steady state and industrially relevant reaction conditions with high product concentration and conversion. Figure 8 demonstrates feed and bleed operation over an extended experimental duration of six hours showing no significant change in FE and conversion after the transient phase. For further improving FE and conversion of methanol oxidation to formate, more selective catalysts are essential, in addition the structure of the present electrode could be improved. Reducing the thickness of the dendrite layer or forcing convective transport into the pores might improve mass transfer into the porous layer.[43] For improved reaction conditions, we would like to refer to our previous publication,[43] which showed that increasing the temperature and decreasing the current density increased FE and conversion. From a process perspective, selective separation of formate from the electrolyte could improve FE and conversion by preventing overoxidation to carbonate. In the context of feed and bleed, selective product removal is beneficial because a concentrated product stream is removed from the system instead of the otherwise nonselective bleed stream. Feed and bleed electrosynthesis of formate could be coupled with a selective separation process such as bipolar membrane electrodialysis[45–48] to investigate the overall process at steady state and industrially relevant conditions.

3. Conclusions

In this study, we explored the "feed and bleed" operating mode for electrosynthesis in flow cells, specifically targeting its utility in lab-scale research. A model was presented to facilitate the understanding and analysis of the behavior of the feed and bleed system in both transient and steady state. A novel 3D-printed phase separator was developed to efficiently tackle gas separation from the electrolyte loop, leveraging gravity and centrifugal forces for effective separation while maintaining a low internal volume. This separator can be reproduced through additive manufacturing techniques using readily accessible materials.

Moreover, we introduced a versatile experimental setup with a low internal volume tailored for the feed and bleed operating mode. The setup's capability to operate in batch and single-pass mode as well enabled a direct comparison of all three operating modes at the example of methanol oxidation to formate. Furthermore, the setup can be employed in future studies to select the operating mode depending on the research question without the need for hardware changes. Online FTIR analytics, featuring a high sampling rate, provided comprehensive insights into the characteristics of each operation mode, offering valuable guidance for researchers in selecting the most suitable operating mode for their experiments. Notably, the comparison highlighted that the feed and bleed mode uniquely supported continuous operation at both steady-state and high conversion levels.

Our study spotlights the advantages of feed and bleed operation in comparison to batch and single-pass modes, solves practical challenges, and provides valuable insights for applying feed and bleed in lab-scale research. The unique characteristics of feed and bleed render it particularly suitable for investigating continuous processes in a steady state over extended periods while maintaining industrially relevant conditions with high product concentration. Beyond the demonstrated setup for liquid product streams, the feed and bleed approach also holds potential for applications involving microfluidic reactors, gaseous product streams, or automated experimentation.

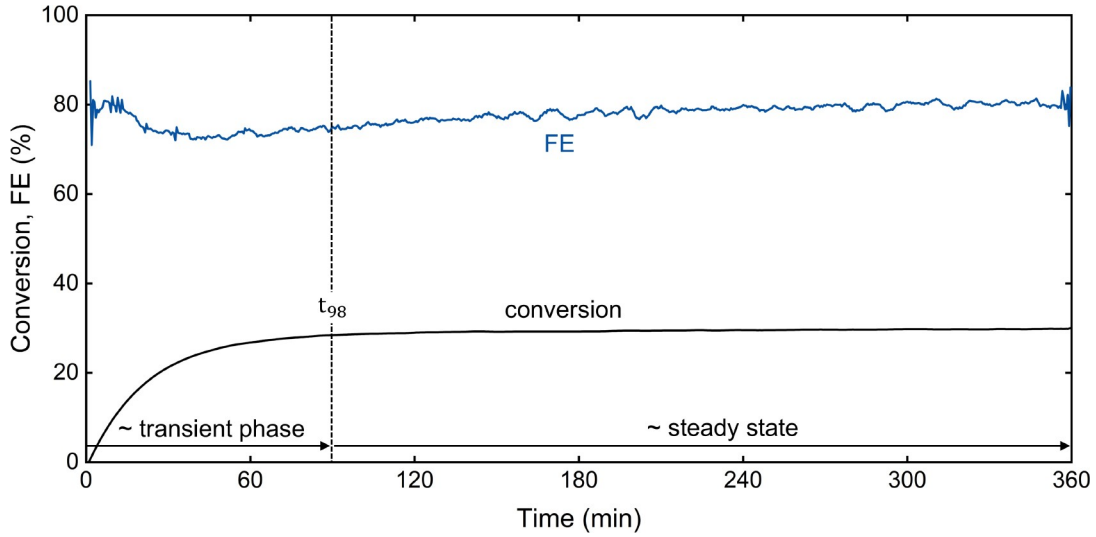

Figure 8. Methanol conversion and the FE for formate plotted over time for an extended experimental duration of six hours. Experimental conditions: 200 mA cm^{-2}, 25 °C, $\dot{V}_{cycle}$ = 50 mL min^{-1}, $\dot{V}_{feed}$ = 2.5 mL min^{-1}, 2 mol L^{-1} KOH, 1 mol L^{-1} methanol.

Materials and Methods

Theoretical Analysis

All feed and bleed equations were derived from a mole balance around the electrolyte in the system, which was assumed to be ideally mixed. Further details on the ideally mixed model and the balance equation are provided in the results Section 2.1. The assumption of ideal mixing of the electrolyte was evaluated by comparison to a non-ideally mixed model (see Supporting Information S1). The feed and bleed models were implemented with Python using the GEKKO Optimization Suite[49] to solve the equations. All other calculations were performed in Excel (Microsoft) and Origin (OriginLab).

Phase Separator

The phase separator was manufactured by 3D printing (printer: Form 3, material: High Temp Resin V2, Formlabs). After printing, the phase separator was thoroughly rinsed with Isopropanol and cured in a "Form Cure" device (Formlabs) at the manufacturer's recommended settings of 80 °C for 120 min. The 3D model of the phase separator is provided in the Supporting Information. The phase separator was connected via three threaded ports for G1/4" tubing connectors and two smaller threaded ports for UNF 1/4" 28G tubing connectors. The material of the phase separator was transparent, allowing to observe the separation chamber during operation. The visibility of the separation chamber was improved by applying a transparent adhesive film on the dull front surface of the phase separator.

Experimental Comparison of Operation Modes

All experiments were performed in an electrochemical flow cell (flex-E-cell, FXC Engineering) with an active geometric area of 5 cm by 5 cm with two electrolyte compartments separated by a bipolar membrane (Fumasep FBM-PK, Fumatech) in reverse bias. The anolyte was an aqueous solution of 2 mol L^{-1} potassium hydroxide (KOH, 85 %, VWR) and 1 mol L^{-1} methanol (CH_3OH, 99.9 %, Merck), the catholyte was a solution of 1 mol L^{-1} potassium hydroxide. The anode was a copper foam (POROFEN-Cu90, AlCarbon) coated with copper(II) oxide dendrites. The anode preparation procedure was adapted with modifications from Huan et al.[50] Anodic methanol oxidation was paired with hydrogen evolution at the cathode, which was a nickel mesh (aperture width 0.5 mm, wire diameter 0.14 mm, Haver & Boecker) supported by copper foam. The electrodes and cell setup were identical to our previous work on methanol oxidation to formate, please refer to our previous publication for further details.[43] The flow cell was operated at constant current supplied by a potentiostat (VSP with 10 A booster, Biologic) at a current density of 200 mA cm^{-2}. Potentials were measured using a reversible hydrogen electrode (RHE)(Hydroflex, Gaskatel).

Figure 9 shows a schematic of the cell and the experimental setup consisting of two separate electrolyte cycles. The electrolytes were circulated with a peristaltic pump (Masterflex L/S Digital, Cole-Parmer) through the electrochemical flow cell and a heat exchanger (flex-H-cell, FXC Engineering). The heat exchanger was connected to a thermostat set to 25 °C. Each electrolyte cycle contained a phase separator (see Section 2.2) for removal of excess volume and gas bubbles, which was connected in short distance after the flow cell outlet. The phase separator allowed operating with a low electrolyte volume without a flask or reservoir within the electrolyte cycle. The total anolyte volume was 56.5 mL, which was determined by measuring the volume of water that fits into the anolyte cycle. To determine the correct electrolyte volume, it should be ensured that the electrolyte cycle is filled completely with water with no remaining air bubbles. A sample stream from the anolyte was circulated at 10 mL min^{-1} through the flow cell probe of an FTIR spectrometer (ReactIR 702 L with Micro Flow Cell, Mettler Toledo). The concentrations of methanol and formate were measured with an FTIR spectrometer at a sample rate of 2 min^{-1}. The concentration data obtained from the spectrometer software (iC-IR, Mettler Toledo) was further processed and analyzed in Origin (OriginLab).

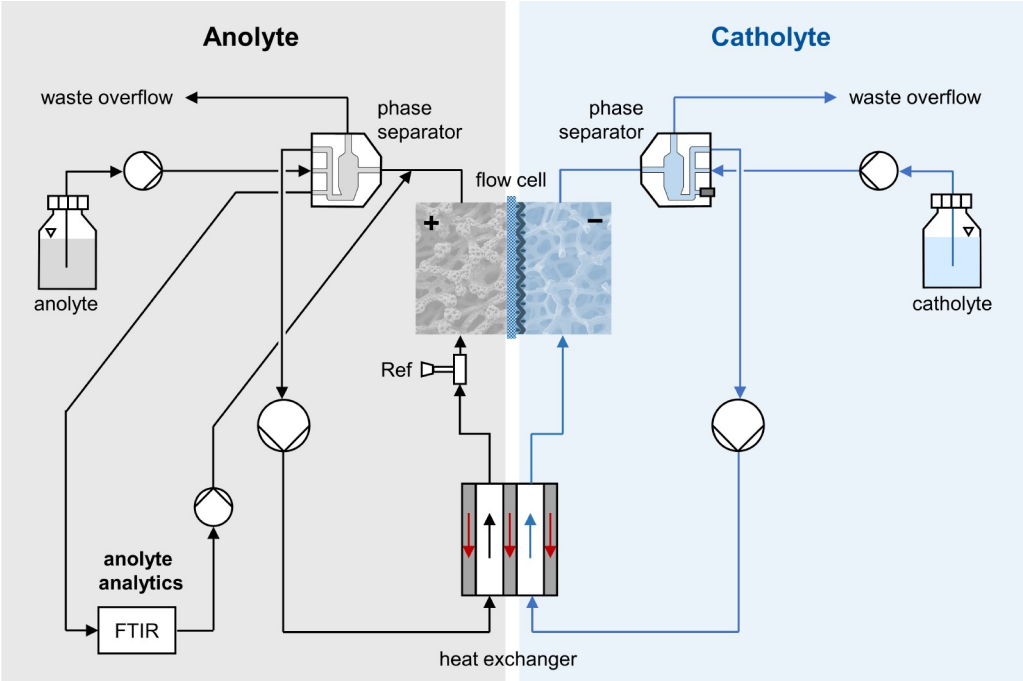

Figure 9. Experimental setup used for batch, single-pass, and feed and bleed mode.

Weighted adjacent averaging with a window size of 20 points was applied to the concentration data, which removed noise from the data without altering the shape of the concentration curves. The conversion of methanol was calculated from the smoothed concentration data according to Equation (9) with the initial methanol concentration $c_{MeOH,0}$ and the current methanol concentration c_{MeOH}.

$$conversion = \frac{c_{MeOH,0} - c_{MeOH}}{c_{MeOH,0}} \quad (9)$$

For further information on the FTIR analytics please refer to our previous publication.[43] The sample stream and the feed stream were supplied by peristaltic pumps (Reglo ICC, Ismatec). For all experiments, the cathode side was operated in feed and bleed mode at a volume flow of 50 mL min^{-1} in the loop and 5 mL min^{-1} for the feed. Detailed pump settings on the anode side for batch, single-pass, and feed and bleed operation are illustrated in Figure S5.

Acknowledgements

M. Wessling acknowledges DFG funding through the Gottfried Wilhelm Leibniz Award 2019 (WE 4678/12-1). This work was conducted in part at the Competence Center Industrial Electrochemistry ELECTRA, which is supported by the European Regional Development Fund (ERDF) and the Federal State of North Rhine-Westphalia (grant no. ERDF 05 00 07 7). This work was supported by the German Federal Ministry of Education and Research (BMBF) within the project iNEW 2.0 (FKZ 03SF0627). The authors thank Miriam Mineur and Nicolas Mulandi for their valuable contribution to the experimental setup and the phase separator. Additionally, J. Baessler thanks the networking program 'Sustainable Chemical Synthesis 2.0' (SusChemSys 2.0) for the support and fruitful discussions across disciplines. Open Access funding enabled and organized by Projekt DEAL.

Conflict of Interests

The authors declare the following financial interests/personal relationships: Jonas Baessler reports a relationship with FXC Engineering GmbH that includes: board membership, employment, and equity or stocks. Jonas Baessler, Matthias Wessling, and Robert Keller have patented "Flusszelle mit verbessertem Aufbau" issued to RWTH Aachen University. The authors declare that they have no other known competing financial interests or personal relationships that could have appeared to influence the work reported in this paper.

Data Availability Statement

The data that support the findings of this study are available from the corresponding author upon reasonable request.

Keywords: electrochemistry · oxidation · electrochemical flow cell · flow reactor · continuous operation with recirculation

[1] M. J. Orella, Y. Román-Leshkov, F. R. Brushett, *Curr. Opin. Chem. Eng.* **2018**, *20* 159.
[2] S. Gu, B. Xu, Y. Yan, *Annu. Rev. Chem. Biomol. Eng.* **2014**, *5* 429.
[3] K. K. Jaiswal, C. R. Chowdhury, D. Yadav, R. Verma, S. Dutta, K. S. Jaiswal, K. S. K. Karuppasamy, et al., *Energy Nexus* **2022**, *7* 100118.
[4] H. Gavin, In *Oxford Energy Colloquia* **2019** .
[5] M. Liao, W. Xu, Y. Song, Z. Pan, H. Zheng, Y. Li, X. Qin, L. Wang, J. Lu, Z. Wang, *Nano Energy* **2023**, *116* 108831.
[6] T. Burdyny, W. A. Smith, *Energy Environ. Sci.* **2019**, *57* 2165.
[7] N. Thissen, J. Hoffmann, S. Tigges, D. A. M. Vogel, J. J. Thoede, S. Khan, N. Schmitt, S. Heumann, B. J. M. Etzold, A. K. Mechler, *ChemElectroChem* **2024**, *11*, 1.
[8] S. C. Perry, D. Pangotra, L. Vieira, L.-I. Csepei, V. Sieber, L. Wang, C. Ponce de León, F. C. Walsh, *Nat. Chem. Rev.* **2019**, *3* (7), 442.
[9] D. Bergner, *J. Appl. Electrochem.* **1982**, *12* (6), 631.
[10] H. Lange, A. Klose, L. Beisswenger, D. Erdmann, L. Urbas, *Sustain. Energy Fuels* **2024**, *8* (6), 1208.
[11] F. F. Rivera, C. P. de León, J. L. Nava, F. C. Walsh, *Electrochim. Acta* **2015**, *163*, 338.
[12] D. Pletcher, R. A. Green, R. C. D. Brown, *Chem. Rev.* **2018**, *118* (9), 4573.
[13] F. C. Walsh, L. F. Arenas, C. Ponce de León, *Curr. Opin. Electrochem.* **2019**, *16* 10.
[14] B. Endrődi, G. Bencsik, F. Darvas, R. Jones, K. Rajeshwar, C. Janáky, *Prog. Energy Combust. Sci.* **2017**, *62* 133.
[15] J.-B. Vennekoetter, R. Sengpiel, M. Wessling, *Chem. Eng. J.* **2019**, *364*, 89.
[16] S. C. Perry, C. Ponce de León, F. C. Walsh, *J. Electrochem. Soc.* **2020**, *167* (15), 155525.
[17] M. Quentmeier, B. Schmid, H. Tempel, H. Kungl, R.-A. Eichel, *ACS Sustainable Chem. Eng.* **2023**, *11* (2), 679.
[18] S. Möhle, M. Zirbes, E. Rodrigo, T. Gieshoff, A. Wiebe, S. R. Waldvogel, *Angew. Chem. Int. Ed.* **2018**, *57* (21), 6018.
[19] H. Shin, S. Lee, Y.-E. Sung, *Curr. Opin. Electrochem.* **2023**, *38*, 101224.
[20] M. Regnier, C. Vega, D. I. Ioannou, T. Noël, *Chem. Soc. Rev.* **2024**, *53* (21), 10741.
[21] L. F. Arenas, C. Ponce de León, F. C. Walsh, *J. Electrochem. Soc.* **2020**, *167* (2), 023504.
[22] O. M. Cornejo, M. F. Murrieta, Z. G. Aguilar, J. F. Rodríguez, A. A. Márquez, M. I. León, J. L. Nava, *Chem. Eng. J.* **2024**, *496*, 153935.
[23] N. Tanbouza, T. Ollevier, K. Lam, *iScience* **2020**, *23* (11), 101720.
[24] S. Maljuric, W. Jud, C. O. Kappe, D. Cantillo, *J. Flow Chem.* **2020**, *10* (1), 181.
[25] T. Noël, Y. Cao, G. Laudadio, *Acc. Chem. Res.* **2019**, *52* (10), 2858.
[26] T. P. Nicholls, C. Schotten, C. E. Willans, *Curr. Opin. Green Sustain. Chem.* **2020**, *26*, 100355.
[27] R. A. Green, R. C. D. Brown, D. Pletcher, B. Harji, *Org. Process Res. Dev.* **2015**, *19* (10), 1424.
[28] D. Pletcher, F. C. Walsh, *Industrial Electrochemistry* **1993**.
[29] F. Goodridge, K. Scott, *Electrochemical Process Engineering* **1995**.
[30] H. Lund, O. Hammerich, *Organic electrochemistry*, Marcel Dekker, New York, NY, 4. ed., Rev. and Expanded. edition, **2001**.
[31] D. E. Danly, *J. Electrochem. Soc.* **1984**, *131* (10), 435 C.
[32] R. W. Baker, *Membrane technology and applications*, John Wiley & Sons, Chichester West Sussex and Hoboken, 3rd ed. edition, **2012**.
[33] M. Cheryan, *Ultrafiltration and microfiltration handbook*, Technomic Pub. Co, Lancaster, Pa., **1998**.
[34] M. S. Mintz, *Ind. Eng. Chem.* **1963**, *55* (6), 18.
[35] M. Rakib, P. Mocoteguy, P. Viers, E. Petit, G. Durand, *J. Appl. Electrochem.* **1999**, *29* 1439.
[36] A. Dominguez-Ramos, A. Irabien, *Ind. Eng. Chem. Res.* **2013**, *52* (22), 7534.
[37] P. Drögemüller, T. Stobbe, U. Schröder, *ChemSusChem* **2024**, *17* (2), e202300973.
[38] M. Li, X. Deng, Y. Liang, K. Xiang, D. Wu, B. Zhao, H. Yang, J.-L. Luo, X.-Z. Fu, *J. Energy Chem.* **2020**, *50*, 314.
[39] X. Wei, Y. Li, L. Chen, J. Shi, *Angew. Chem. Int. Ed.* **2021**, *60* (6), 3148.
[40] K. Xiang, Z. Song, D. Wu, X. Deng, X. Wang, W. You, Z. Peng, L. Wang, J.-L. Luo, X.-Z. Fu, *J. Mater. Chem. A* **2021**, *9* (10), 6316.
[41] J. Baessler, T. Oliveira, R. Keller, M. Wessling, *ACS Sustainable Chem. Eng.* **2023**, *11* (18), 6822.
[42] F. Schwarz, E. Larenz, A. K. Mechler, *Green Chem.* **2024**.

[43] J. Baessler, N. Vollmert, J. Vehrenberg, M. Mineur, S. Schenke, L. Griesberg, P. M. Pineda, R. Keller, *Chem. Eng. J.* **2024**, *495* 153000.
[44] H. Heli, M. Jafarian, M. G. Mahjani, F. Gobal, *Electrochim. Acta* **2004**, *49* (27), 4999.
[45] M. Ramdin, A. R. T. Morrison, M. de Groen, R. van Haperen, R. de Kler, E. Irtem, A. T. Laitinen, L. J. P. van den Broeke, T. Breugelmans, J. P. M. Trusler, W. de Jong, T. J. H. Vlugt, *Ind. Eng. Chem. Res.* **2019**, *58* (51), 22718.
[46] A. Kaur, B. Kim, R. Dinsdale, A. Guwy, E. Yu, G. Premier, *J. Chem. Technol. Biotechnol.* **2021**, *96* (9), 2461.
[47] X. Wei, Y. Wang, H. Yan, C. Jiang, T. Xu, *Sep. Purif. Technol.* **2021**, *254*, 117563.
[48] Z. Wang, J. Yan, H. Wang, W. Fu, D. He, B. Wang, Y. Wang, T. Xu, *J. Membr. Sci.* **2024**, *708*, 123016.
[49] L. Beal, D. Hill, R. Martin, J. Hedengren, *Processes* **2018**, *6* (8), 106.
[50] T. N. Huan, G. Rousse, S. Zanna, I. T. Lucas, X. Xu, N. Menguy, V. Mougel, M. Fontecave, *Angew. Chem. Int. Ed.* **2017**, *56* (17), 4792.

Manuscript received: January 27, 2025
Revised manuscript received: February 24, 2025
Version of record online: ■■, ■■

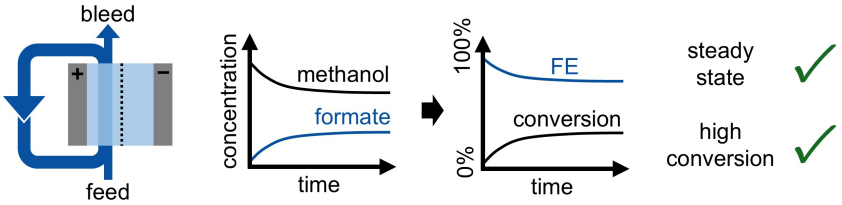

Continuous “feed and bleed” operation is introduced as a versatile alternative to conventional batch recirculation and single-pass operation modes for electrochemical synthesis in flow cells. ‘Feed and bleed’ is demonstrated by electrochemical methanol oxidation to formate, showcasing its unique characteristics, which enable steady state operation with high conversion at industrially relevant conditions.

*J. Baessler, M. Wehner, M. Mohseni, J. Neumann, M. Wessling, R. Keller**

1 – 12

Feed and Bleed Operating Mode for Electrochemical Flow Cells: Challenges, Solutions and Practical Insights